Nanoparticle manipulation using plasmonic optical tweezers based on particle sizes and refractive indices

HUAXIN LI,[1,2] **YATAO REN,**[1,2,3,*] **YANG LI,**[1] **MINGJIAN HE,**[1,2] **BAOHAI GAO,**[1,2] **AND HONG QI**[1,2,4]

[1] *School of Energy Science and Engineering, Harbin Institute of Technology, Harbin 150001, China*
[2] *Key Laboratory of Aerospace Thermophysics, Ministry of Industry and Information Technology, Harbin 150001, China*
[3] *Faculty of Engineering, University of Nottinghamhttps://ror.org/01ee9ar58, University Park, Nottingham NG7 2RD, UK*
[4] *qihong@hit.edu.cn*
[*] *renyt@hit.edu.cn*

Abstract: As an effective tool for micro/nano-scale particle manipulation, plasmonic optical tweezers can be used to manipulate cells, DNA, and macromolecules. Related research is of great significance to the development of nanoscience. In this work, we investigated a sub-wavelength particle manipulation technique based on plasmonic optical tweezers. When the local plasmonic resonance is excited on the gold nanostructure arrays, the local electromagnetic field will be enhanced to generate a strong gradient force acting on nanoparticles, which could achieve particle sorting in sub-wavelength scale. On this basis, we explored the plasmonic enhancement effect of the sorting device and the corresponding optical force and optical potential well distributions. Additionally, the sorting effect of the sorting device was investigated in statistical methods, which showed that the sorting device could effectively sort particles of different diameters and refractive indices.

1. Introduction

Optical tweezer is a noninvasive and versatile tool for manipulating microscale objects [1–3]. It has attracted wide attention since being proposed in 1986 by Arthur Ashkin [4], who was awarded the Noble Prize in Physics in 2018. Traditional optical tweezer technology uses a highly focused laser to generate gradient force to manipulate particles [5]. Due to the diffraction limit, it is difficult to be used to manipulate objects below the sub-wavelength range. Meanwhile, high-precision particle manipulation using traditional optical tweezers usually requires high laser power, which may cause irreversible damage to heat-sensitive objects such as DNA and proteins [6]. Recently, it was found that the near-field optical manipulation based on surface plasmon resonance has the potential to overcome above limitations. In this method, the gradient force acting on objects is generated by the enhanced electromagnetic field, which stems from localized surface plasmon resonance. Due to the strong near-field enhancement, particles can be manipulated at a lower laser power and the spatial resolution can be improved beyond the diffraction limit at the same time [7,8].

When the surface plasmon resonance of metal nanoparticles is excited, a significant near-field enhancement will be produced. This kind of enhancement of metal nanoparticles has a wide application in the field of chemistry, biology, and material, etc. [9–14]. It has been shown that this local field enhancement effect is related to the size, shape, and components of the particles

and the properties of the surrounding medium [15]. On this basis, different plasmonic structures have been applied to obtain different functions [16–20]. With the development of nanofabrication technology, complex nanostructures could be fabricated by self-assembly, lithography, etching, etc., which makes nanoarrays of great interest [21–25]. Unlike the resonances of individual plasmonic structures, the resonances of nanoparticle arrays have higher resonance peaks due to the interaction between particles [26]. Meanwhile, the electromagnetic field enhancement is affected by the array shape, arrangement, and polarization direction of the incident light [27]. Therefore, different kinds of optical tweezers based on nanostructure arrays have been developed to achieve different functions. Examples include the use of surface-enhanced Raman spectroscopy [28,29] and particle sorting [30].

As a popular application of plasmonic optical tweezers, particle sorting is an important application of the central process of many areas of nanoscience and technology, such as 'lab-on-chip' technology. Commonly used sorting methods include chromatography, electrophoresis, and field-flow fractionation, etc. [31–33]. While these widely used methods do not facilitate miniaturization and dynamic configuration, which means difficult to sort particles on the chip. To address this issue, optical manipulation is regarded as a promising technology for optofluidic chip sorting due to its high spatial resolution, high integration, and the feasibility of dynamic configuration [34]. Over the last few years, different kinds of sorting devices based on optical manipulation have been designed. For instance, Shi et al. designed a kind of particle sorting device which can achieve shape-selective sieving [30]. The device consists of an optofluidic sawtooth array that can generate sawtooth-like light. Particles with different shapes will be affected by different optical torques. On this basis, the device can enable the sorting of spherical and rod-shape bacteria with a sorting rate of over 95%. Xu et al. designed an optical particle sorting platform on a silicon-based chip system that enables multilevel sorting of particles [35]. By adjusting the optical power ratio between the parallel waveguides, four-level sorting of particles with a diameter over 300 nm can be achieved. Yang et al. experimentally realized carbon nanotubes removal by dipping the tapered fiber tip into the carbon nanotube suspension [36]. Under 1550 nm laser illumination, there will be obvious thermal convection near the tip due to the temperature gradient generated by the photothermal effect. The dispersed carbon nanotubes accumulated firmly on the fiber tip via convection. However, there are few reports on the optical sorting of particles with different diameters and refractive index below 100 nm.

Here, we present a particle sorting device using plasmonic optical tweezers, which can realize automatic sorting based on particle size and refractive index. We initially explored the local field enhancement of the nanostructure and the optical force generated by the nanostructure. Simulation is performed by COMSOL Multiphysics based on the finite element method. Additionally, the sorting effect of the sorting device was investigated in statistical methods, with Brownian force and viscous resistance under consideration. A Fortran code is developed to calculate the optical potential well and particle capture rate by solving Eq. (5) and Eq. (6). For particles of a certain diameter or refractive index, the capture rate can be over 90%. Furthermore, the nanostructure arrays are conducive to large-scale integration in microfluidic chips due to the simplicity of combination.

2. Methods

2.1. Maxwell stress tensor method

The optical forces acting on a particle in the electromagnetic field can be divided into two parts: scattering force and gradient force. The scattering force is the optical radiation pressure that pushes particles along the direction of the incident light. The gradient force is generated by the light field gradient. The direction of the gradient force points to the focus [37]. Maxwell stress tensor method is commonly used to obtain the optical force. By defining the Maxwell tensor in the electromagnetic field, the magnitude of the light force can be obtained by integrating on the

surface of the object. The optical force obtained by this method is the sum of scattering force and gradient force. The stress tensor can be expressed as [38]:

$$\mathbf{T} = \left[\varepsilon_0 \mathbf{EE} + \mu_0 \mathbf{HH} - \frac{1}{2}(\varepsilon_0 E^2 + \mu_0 H^2)\mathbf{I} \right],$$ (1)

where $\mathbf{E}$ is the electric field intensity, $\mathbf{H}$ is the magnetic field intensity, ε_0 is the permittivity of the medium, μ_0 is the magnetic permeability of the medium, and $\mathbf{I}$ is the third-order unit tensor. The stress tensor is a symmetric tensor, which can be expressed as [38]:

$$\mathbf{T} = \begin{bmatrix} \varepsilon_0 E_1^2 + \mu_0 H_1^2 - \frac{1}{2}(\varepsilon_0 E^2 + \mu_0 H^2 & \varepsilon_0 E_1 E_2 + \mu_0 H_1 H_2 & \varepsilon_0 E_1 E_3 + \mu_0 H_1 H_3 \\ \varepsilon_0 E_2 E_1 + \mu_0 H_2 H_1 & \varepsilon_0 E_2^2 + \mu_0 H_2^2 - \frac{1}{2}(\varepsilon_0 E^2 + \mu_0 H^2) & \varepsilon_0 E_1 E_3 + \mu_0 H_1 H_3 \\ \varepsilon_0 E_3 E_1 + \mu_0 H_3 H_1 & \varepsilon_0 E_3 E_2 + \mu_0 H_3 H_2 & \varepsilon_0 E_3^2 + \mu_0 H_3^2 - \frac{1}{2}(\varepsilon_0 E^2 + \mu_0 H^2) \end{bmatrix}.$$ (2)

The optical force acting on particles in the electromagnetic field is [39]:

$$\mathbf{F} = \oiint \langle \mathbf{T} \rangle \cdot \mathbf{n} dS.$$ (3)

According to the electromagnetic field distribution obtained, the optical force acting on particles can be calculated by Eq. (3). When the optical force distribution of a certain particle is obtained, the optical potential well depth at r_0 can be calculated by [40]:

$$U(r_0) = \int_\infty^{r_0} F(r) dr.$$ (4)

The potential well depth represents the capture stability of particles. A large potential well depth means it can capture particles stably. In order to trap a nanoparticle, the minimum of the potential well is 1 $k_{\mathrm{B}}T$, where k_{B} is the Boltzmann constant, and T is the absolute temperature [41]. When the potential well is shallower than 1 $k_{\mathrm{B}}T$, the nanoparticle can easily hop away from the potential well.

2.2. Particle capture probability

For multiple particles, the effect of particle capture can be denoted by capture probability, which is the probability that a particle is captured at a certain location. In this work, capture probability is obtained by statistical methods, which simulate the movement of a large number of particles and count the number of captured and escaped particles. In the microchannel, suspended particles are affected by optical force, fluid viscosity resistance, and Brownian force. So the one-dimensional motion equation of particles can be expressed as [15]:

$$F_{\mathrm{op}} + F_{\mathrm{Br}} - F_{\mathrm{drag}} = m_{\mathrm{p}} \frac{d^2 x}{dt^2},$$ (5)

where F_{op} is the optical force, F_{Br} is the Brownian force, F_{drag} is the viscous resistance, m_{p} is the particle mass, and x is the particle displacement over time. Brownian force and viscous resistance can be calculated as [15]:

$$F_{\mathrm{drag}} = 6\pi R_0 \eta v,$$ (6)

$$F_{\mathrm{Br}} = R\sqrt{\frac{12\pi k_B T R_0 \eta}{\Delta t}},$$ (7)

where R_0 is the radius of the particle, η is the dynamic viscosity of water, and v is the instantaneous velocity of the particle. R is a random number with Gauss distributed, with a mean value of 0 and a variance of 1. T is the temperature, and the surrounding temperature is 300 K. Δt is the time

interval of Brownian force action. When Brownian force is integrated within a long period of time t ($t >> \Delta t$), the choice of the time interval is independent of particle motion, and Brownian force is considered to be a constant value within each time interval. Therefore, the equation of particle motion at the ith time interval can be written as:

$$F_{op} + F_{Br} - 6\pi\eta R_0 v = m_p \frac{dv}{dt}.$$

(8)

Therefore, the instantaneous velocity of the particle is [42]:

$$v_i = \left(v_{i-1} - \frac{F_{op} + F_{Br}}{6\pi\eta R_0}\right)\exp\left(-\frac{6\pi\eta R_0}{m}\Delta t\right) + \frac{F_{op} + F_{Br}}{6\pi\eta R_0},$$

(9)

The particle displacement at a time interval is [42]:

$$x_i - x_{i-1} = \int_0^{\Delta t} v dt = \frac{m_p}{6\pi\eta R_0}\left(v_{i-1} - \frac{F_{op} + F_{Br}}{6\pi\eta R_0}\right)\left[1 - \exp\left(-\frac{6\pi\eta R_0}{m}\Delta t\right)\right] + \frac{F_{op} + F_{Br}}{6\pi\eta R_0}\Delta t. \quad (10)$$

Then, the particle displacement within a certain time range can be calculated. By increasing the number of particles, the particle displacement and distribution after a period of time can be calculated, so as to obtain the capture probability of the particle.

3. Results and discussion

In this section, we investigated the optical force distribution around the nanostructure and its influencing factors. On this basis, a nanoparticle sorting device is designed based on plasmonic optical tweezers. One-dimensional array of four cuboid gold nanoparticles is placed on a glass substrate with water as the surrounding medium. The polarization direction of the incident laser can be controlled by a polarizer. Due to the laser irradiation, the local enhanced electromagnetic field is formed in the gap of the nanostructure, which has the effect of trapping force on the nanoparticles. The electromagnetic field distribution was calculated by integrating Maxwell tensor on the surface of nanoparticles with Eq. (3). By moving the position of the nanoparticles, the optical force distribution around the nanostructure can be obtained, then the optical potential well depth can be obtained by integrating the optical force with Eq. (4). Finally, the capture probability can be obtained by simulating the motion of a large number of particles, which can reflect the sorting effect of the sorting device.

3.1. Local electric field enhancement of nanostructures

As shown in Fig. 1, the gold nanostructure array is arranged on SiO_2 substrate in the same direction as the laser polarization direction. The laser power density is set as 5×10^9 W/m^2, cuboid length $l = 226$ nm, width $d = 80$ nm, height $h = 40$ nm. The incident direction of laser is along the negative direction of the z-axis, and the laser is polarized along the x-axis. The dielectric function of gold is obtained from Ref. [15].

In order to select the appropriate gap distance, the effect of gap distance on the field enhancement at different incident wavelengths was investigated. It can be seen from Fig. 2 that the field enhancement increases with the decrease of the gap distance. For the wavelengths longer than 800 nm, the field enhancement at location A is obvious, while it increases significantly for the wavelengths longer than 1100 nm at location B. When the gap distance $s = 20$ nm, the electromagnetic field enhancement at both locations dramatically increases, which can reach more than 40 with wavelengths longer than 1700nm.

The above results show the local field enhancement at the center of the gap of the nanostructure. On this basis, taking wavelength 1400 nm as an example, the electric field enhancement distribution within 100 nm directly above locations A and B is calculated, as described in Fig. 3.
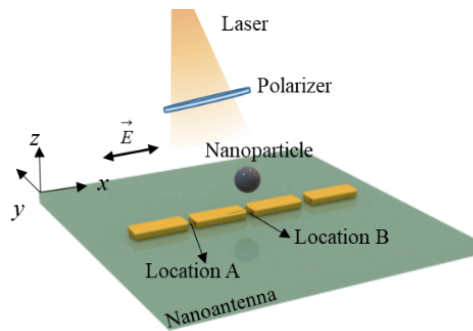
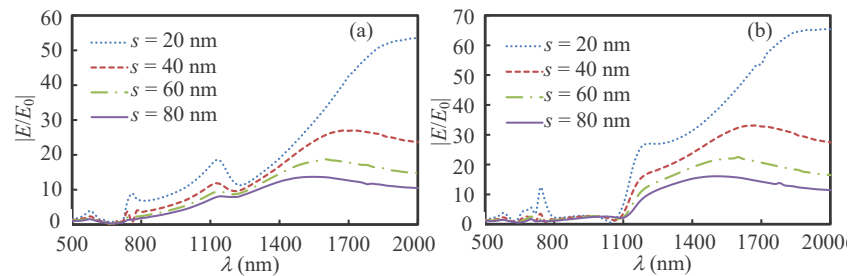**Fig. 1.** Schematic of the nanostructure array

Fig. 2. Field enhancement at different gap distances and wavelengths (a) location A; (b) location B

It can be seen that a smaller gap distance can increase the field enhancement. While the field enhancement decreases fast when it is away from the center, which means the scope of optical capture force is smaller.
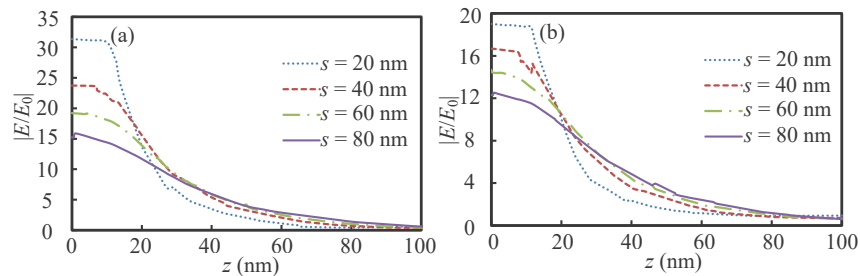

Fig. 3. Enhancement attenuation of the field above the nanostructure with different gap distances (a) location A; (b) location B

In order to determine the incident wavelength, we obtained the field enhancement for different incident wavelengths. As shown in Fig. 4(a), when the wavelength is shorter than 1160 nm, the electric field enhancement at location A is greater than that at location B. When the wavelength is larger than 1160 nm, the electric field enhancement at location A is weaker than that at location B. Taking wavelengths $\lambda = 1064$ nm and 1400 nm, for example, the field enhancement distributions around the nanostructure are shown in Fig. 4(b) and (c). When the wavelength $\lambda = 1064$ nm, the enhancement of the local field around the outer nanoparticles is more obvious, while when the incident wavelength $\lambda = 1400$ nm, the enhancement of the local field around the

inner nanoparticles is larger. This is caused by the different electromagnetic field enhancements at different locations, just as shown in Fig. 4(a).
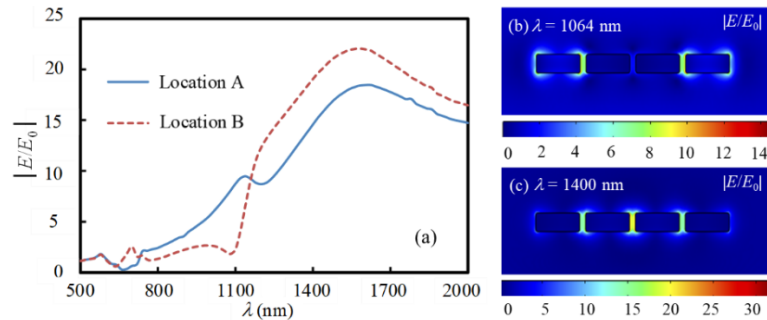

Fig. 4. When gap distance $s = 30$ nm, (a) Electromagnetic field enhancement at different incident wavelengths; (b) Electric field distribution at $\lambda = 1064$ nm; (c) Electric field distribution cloud at $\lambda = 1400$ nm

3.2. Optical force induced by plasmonic nanostructures

The optical force acting on the nanoparticle is obtained by integrating the Maxwell tensor over the surface of the target nanoparticle. The distribution of the optical force around the plasmonic nanostructure is obtained by moving the nanoparticle's position. The distribution of the optical force around the plasmonic nanostructure is obtained by moving the nanoparticle's position with a 10 nm step size. Meanwhile, the potential well distribution is obtained by integrating the optical force along x-direction. The gap distance of the nanostructure is 30 nm. The diameter of the captured spherical nanoparticles is set as $D = 100$ nm, refractive index $n = 2$. The lowest point of the captured nanoparticles is 10 nm above the nanostructure. We firstly investigated the distribution of optical force and optical well with laser wavelength $\lambda = 1400$ nm.

When the force in a certain direction is zero, the nanoparticle is in force equilibrium in this direction. By analyzing the optical force in Fig. 5(a) and the potential well in Fig. 5(b), there are five stable capture points in the x-direction, as shown in Fig. 5(a). The three capture points of the array gap are more stable. Similarly, the capture point in the y-direction is the gap center of the structure. The force in the y-direction is always negative, indicating an attraction to the particles above it. The above results indicate that the gaps of the array nanostructures have forces that can be used for optical trapping of nanoparticles in x, y, and z directions.

As a comparison, the optical force and the potential well distribution with the laser wavelength $\lambda = 1064$ nm were calculated. Different from the results of $\lambda = 1400$ nm, there are two adjacent stable capture points on each side (see Fig. 6(a)). The width of the potential well is larger, indicating that the trapping range of the potential well is larger. It can be seen from Fig. 6(d) that there is weak repulsion for nanoparticles in the middle of the nanostructure, and only the outer gap of the array can capture the nanoparticles. Meanwhile, the optical force and the potential well depth are smaller than those in wavelength 1400 nm.

3.3. Influence factors of optical capture force

The above results are based on particles with a fixed property. In this section, the incident laser wavelength is set as 1400 nm. The effects of the diameter D of nanoparticles, the refractive index n, and the vertical distance L_z to the surface of the nanostructure on the optical force were investigated. As shown in Fig. 7, with the increase of L_z, the force decreases gradually. When L_z is larger than 50 nm, the optical force tends to zero, indicating that the nanostructure has a
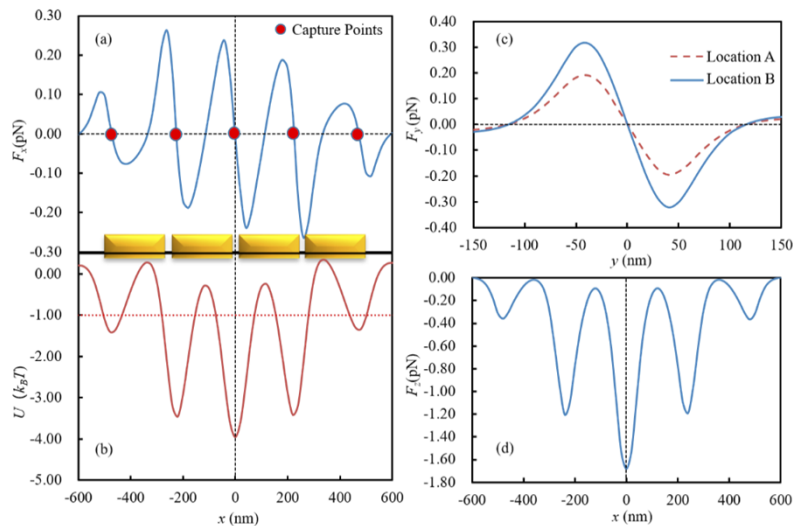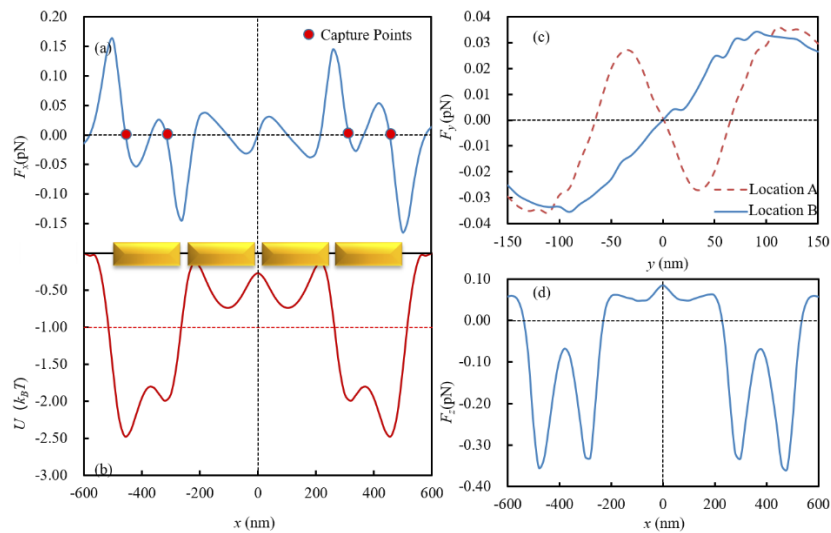
Fig. 5. As $\lambda = 1400$ nm, optical force and potential well distribution for a nanosphere with diameter 100 nm and refractive index $n = 2$ above the array. (a) optical force along x-direction; (b) potential well along x-direction; (c) optical force along y-direction; (d) optical force along z-direction

Fig. 6. As $\lambda = 1064$ nm, optical force and potential well distribution for a nanosphere with diameter 100 nm and refractive index $n = 2$ above the array. (a) optical force along x-direction; (b) potential well along x-direction; (c) optical force along y-direction; (d) optical force along z-direction.

vertical limitation on the capture of nanoparticles, outside which the influence of optical force is negligible.
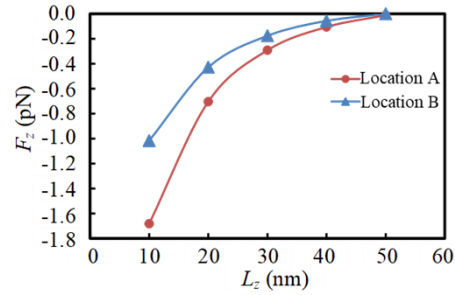

Fig. 7. The optical force in the *z*-direction at different particle heights

When the lowest point of the nanoparticles is 10 nm above locations A and B, the *z*-component of optical force acting on nanoparticles with different diameters *D* and refractive index *n* was obtained. As shown in Fig. 8, with the increase of *D* and *n*, the optical force acting on particles in the *z*-direction increases. The difference is that the optical force increases linearly when *D* increases, while the change rate decreases with the increase of the refractive index. This is because the optical force has a limited range of action, and as the nanoparticles grow larger, the field gradient only acts on part of the particle.
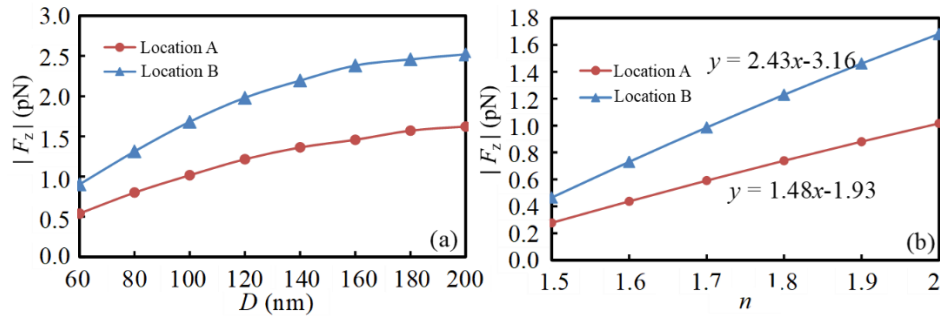

Fig. 8. The optical force in the *z*-direction at different particle diameter *D* and refractive *n*

3.4 Thermophoretic forces around nanostructures

Due to the Joule loss of metals, surface plasmonic on metal nanostructures could generate strong thermal effects. Under the effect of the temperature gradient, thermophoretic force will act on nanoparticles, which can be expressed as [42]:

$$\mathbf{F}_{\mathrm{tp}} = -\frac{6\pi d_{\mathrm{p}} \mu^2 C_{\mathrm{s}} \Lambda \nabla T}{\rho(2\Lambda + 1)T}, \quad \Lambda = \frac{k}{k_{\mathrm{p}}} \tag{11}$$

where *k* is the thermal conductivity of the fluid, k_{p} is the thermal conductivity of the particle, μ is the dynamic viscosity of the fluid, ρ is the density of fluid. From Eq. (11), it can be seen that the thermophoresis force is proportional to the temperature gradient and is related to the thermal conductivity of particles.

In order to obtain the effect of the thermophoresis force on particle trapping, we first calculated the temperature field of the array nanostructure under the laser mentioned above, and the results

are shown in Fig. 9(a). Take carbon nanotubes (CNT) and silicon nanoparticles as examples, the thermophoretic force distributions in the y direction are calculated. The results are shown in Fig. 9(b).
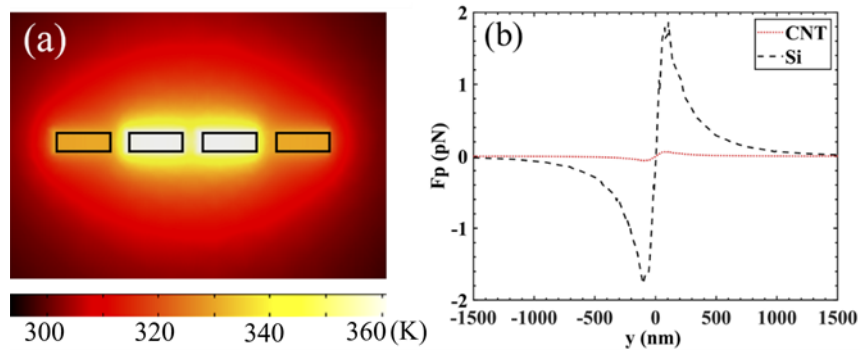

Fig. 9. (a) Temperature field of the array nanostructure; (b) thermophoretic force distributions in the y direction

It can be seen that for nanoparticles with high thermal conductivity, the thermophoresis force has little effect on them. The capture of CNTs has a wide application prospect in biomedicine [36]. In this study, the thermophoresis is ignored based on this situation and further investigations are needed for the manipulation of high thermal conductivity particles such as silicon nanoparticles.

3.5 Particle sorting device with nanostructure array

From the above analysis, it is clear that the main factors affecting the optical force on the particles are the particle diameter and the refractive index. Based on this, an optical sorting device based on nanostructure is designed (see Fig. 10). It consists of three rows of nanoarray with increasing gap distance which is set as 20 nm, 30 nm, and 40 nm successively. The size of the nanostructure is $l = 226$ nm, $d = 80$ nm, and $h = 40$ nm. Particle sorting is achieved when particles of different properties pass through the nanostructure at a certain speed above the intermediate gap, different particles are captured at different gaps under different forces. The incident wavelength is set as 1400 nm. The laser power density is set as 2×10^{10} W/m². From the previous results, it is obvious that the array gap is the capture point at this wavelength. When the captured particle deviates from the gap center in the x-direction, it will still return to the gap center under the action of optical force. Therefore, only the case of particles passing through the center of the array was considered.
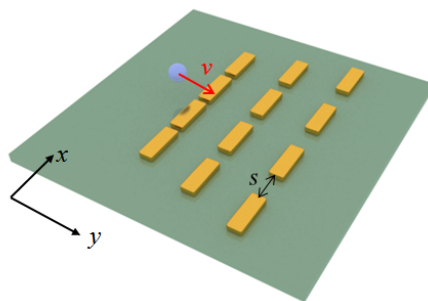

Fig. 10. Schematic diagram of the sorting device

In order to sort particles with different refractive indices, the refractive index of target particles is set as 1.5, 1.6, 1.7, 1.8, 1.9, and 2.0, respectively. The diameter of the particles is set as 100 nm, and the minimum distance from the upper surface of the nanostructure is 10 nm. The optical force acting on particles was calculated every 10 nm. Figure 11 shows the distribution of the optical force acting on the particles with different refractive indices. With the increase of the refractive index, the optical force on the particles increases. For the particles with a certain refractive index, the optical force through the three rows of nanostructures increases successively.
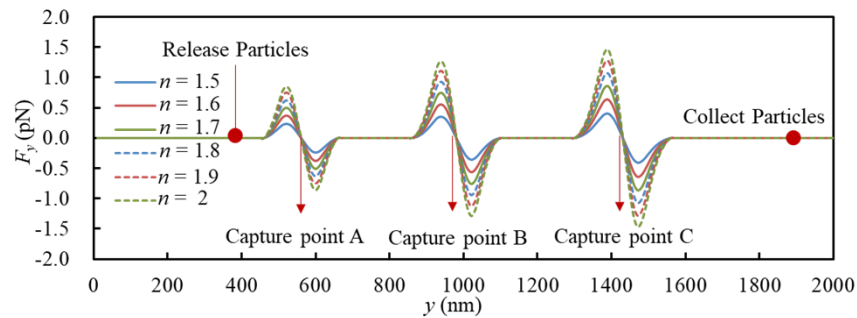

Fig. 11. Optical force distribution of particles with different refractive indices

In order to obtain the statistical results for particle sorting, the particles are released at position $y = 400$ nm with an initial velocity of $v = 100$ nm/s. The particle collection point is set at $y = 1880$ nm to collect the particles that pass through three capture points. In this section, the capture rate is calculated using a statistical method. 200 particles of each type are released, which means the same release situation will be running 200 times. The capture rate can be obtained by recording the position where each particle is captured. It can be seen from Fig. 12 that only particles with refractive index $n = 1.5$ can pass through the sorting device with a passing rate of 79.5%. Therefore, if the particles with different refractive indices are mixed and passed through the sorting device, all particles with refractive index $n = 1.5$ can be collected at the collection point. 97% of particles with refractive index $n = 2$ were captured at location A. As the refractive index of particles decreases, more particles pass through the first nanostructure and are captured by the following capture points. By using this sorter, single or multiple sorting can remove particles with refractive indices in a certain range.

For particles with different diameters, the refractive index of particles was set as $n = 2$. The particle diameter was set as 30 nm, 50 nm, 70 nm, 90 nm, and 110 nm, and other settings were the same as above. Figure 13 shows the optical force distribution of particles with different diameters passing through three nanostructures. As the particle diameter increases, the optical force increases at all three locations. For particles with a certain diameter, the optical force increases as particles pass through three nanostructures. Figure 14 shows the statistical distribution of particles with different diameters through the sorting device. All particles with a diameter of $D = 30$ nm pass through the device and are collected at the particle collection point. The capture rate of particles with diameter $D = 110$ nm at capture position A is 100%. As the particle diameter increases, more particles are trapped by the nanostructure in front. As shown in Fig. 14, particles with diameters of 30 nm, 90 nm, and 110 are densely distributed, with more than 90% of particles captured at the same location. Therefore, the sorter can be used to screen particles with different diameters.
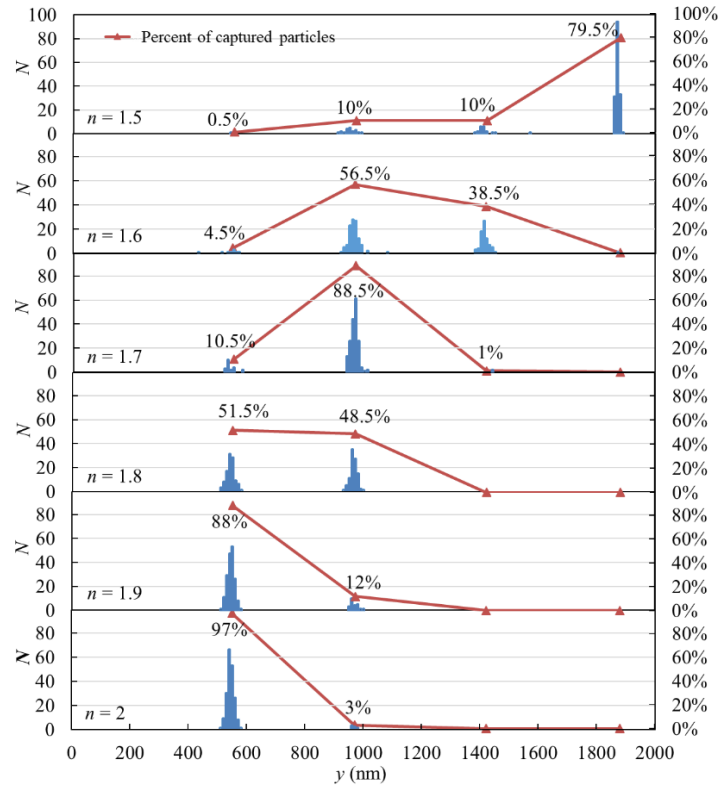
Fig. 12. Statistical distribution and capture rate of particles with different refractive indexes at each capture position
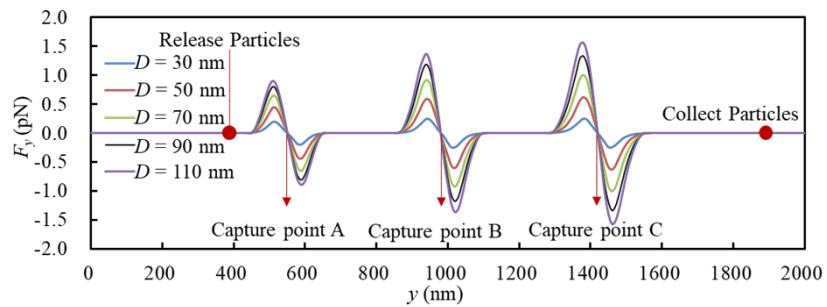

Fig. 13. Optical force distribution of particles with different diameters
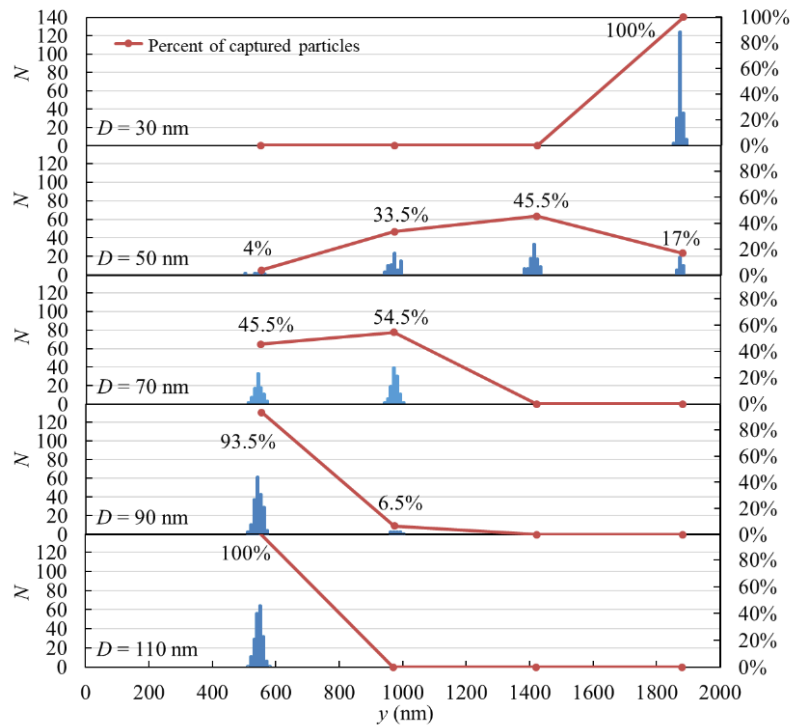
Fig. 14. Statistical distribution and capture rate of particles with different diameters at each capture position

4. Conclusions

In this work, the localized electromagnetic field enhancement and the optical force generated by the nanostructures array are investigated. The nanostructures produce obvious local field enhancement at the gap of the array. On this basis, the influence of gap distance and laser wavelength on the electric field enhancement at the gap is investigated. Reducing the gap distance will increase the field enhancement of the gap, while the area of field enhancement will decrease at the same time. By using the Maxwell stress tensor method, we obtained the optical force distribution and optical potential well distribution of nanostructures. In addition, it is found that the optical force increased with the size of the captured nanoparticles. Similarly, with the increase of the refractive index of nanoparticles, the optical force increases. On this basis, we designed an optical sorting device based on gold nanoarrays. Particles with different sizes and refractive indices have different capture probabilities for different structures, so that particle sorting can be realized under certain conditions. Furthermore, nanoparticles with a certain refractive index or diameter can be removed by changing the laser power density and the gap distance of the array.

Disclosures. The authors declare no conflicts of interest.

Data availability. Data underlying the results presented in this paper are not publicly available at this time but may be obtained from the authors upon reasonable request.

References

1. J. R. Moffitt, Y. R. Chemla, S. B. Smith, and C. Bustamante, "Recent advances in optical tweezers," Annu. Rev. Biochem. **77**(1), 205–228 (2008).
2. I. Prada, L. Amin, R. Furlan, G. Legname, C. Verderio, and D. Cojoc, "A new approach to follow a single extracellular vesicle–cell interaction using optical tweezers," BioTechniques **60**(1), 35–41 (2016).
3. A. Lisica and S. W. Grill, "Optical tweezers studies of transcription by eukaryotic RNA polymerases," Biomol. Concepts **8**(1), 1–11 (2017).
4. A. Ashkin, J. M. Dziedzic, J. E. Bjorkholm, and S. Chu, "Observation of a single-beam gradient force optical trap for dielectric particles," Opt. Lett. **11**(5), 288–290 (1986).
5. D. G. Grier, "A revolution in optical manipulation," Nature **424**(6950), 810–816 (2003).
6. D. G. Kotsifaki, M. Kandyla, and P. G. Lagoudakis, "Plasmon enhanced optical tweezers with gold-coated black silicon," Sci. Rep. **6**(1), 26275 (2016).
7. D. B. Ritchie and M. T. Woodside, "Probing the structural dynamics of proteins and nucleic acids with optical tweezers," Curr. Opin. Struct. Biol. **34**, 43–51 (2015).
8. M. L. Juan, M. Righini, and R. Quidant, "Plasmon nano-optical tweezers," Nat. Photonics **5**(6), 349–356 (2011).
9. E. Kazuma, J. Jung, H. Ueba, M. Trenary, and Y. Kim, "Real-space and real-time observation of a plasmon-induced chemical reaction of a single molecule," Science **360**(6388), 521–526 (2018).
10. B. Schreiber, D. Gkogkou, L. Dedelaite, J. Kerbusch, R. Hübner, E. Sheremet, D. R. T. Zahn, A. Ramanavicius, S. Facsko, and R. D. Rodriguez, "Large-scale self-organized gold nanostructures with bidirectional plasmon resonances for SERS," RSC Adv. **8**(40), 22569–22576 (2018).
11. Z. Yu, M. E. Smith, J. Zhang, Y. Zhou, and P. Zhang, "Determination of trichloroethylene by using self-referenced SERS and gold-core/silver-shell nanoparticles," Microchim. Acta **185**(7), 1–7 (2018).
12. Y. Zhang, J. Wang, J. Shen, Z. Man, W. Shi, C. Min, G. Yuan, S. Zhu, H. P. Urbach, and X. Yuan, "Plasmonic hybridization induced trapping and manipulation of a single Au nanowire on a metallic surface," Nano Lett. **14**(11), 6430–6436 (2014).
13. J. P. Sun, Y. T. Ren, Z. X. Liu, M. J. He, B. H. Gao, and H. Qi, "Dependence of the nonlinear photoacoustic response of gold nanoparticles on the heat-transfer Process," J. Phys. Chem. C **126**(7), 3489–3501 (2022).
14. Y. Ren, H. Qi, Q. Chen, Y. Li, and L. Ruan, "Optofluidic control using light illuminated plasmonic nanostructure as microvalve," Int. J. Heat Mass Transfer **133**, 1019–1025 (2019).
15. Y. Ren, Q. Chen, M. He, X. Zhang, H. Qi, and Y. Yan, "Plasmonic optical tweezers for particle manipulation: principles, methods, and applications," ACS Nano **15**(4), 6105–6128 (2021).
16. J. H. Kang, K. Kim, H. S. Ee, Y. H. Lee, T. Y. Yoon, M. K. Seo, and H. G. Park, "Low-power nano-optical vortex trapping via plasmonic diabolo nanoantennas," Nat. Commun. **2**, 1 (2011).
17. K. Wang and K. B. Crozier, "Plasmonic trapping with a gold nanopillar," ChemPhysChem **13**(11), 2639–2648 (2012).
18. J. P. Zheng, X. B. Xing, J. X. Yang, K. Z. Shi, and S. L. He, "Hybrid optofluidics and three-dimensional manipulation based on hybrid photothermal waveguides," NPG Asia Mater. **10**(4), 340–351 (2018).
19. F. Nan and Z. J. Yan, "Silver-nanowire-based interferometric optical tweezers for enhanced optical trapping and binding of nanoparticles," Adv. Funct. Mater. **29**(7), 1080258 (2019).
20. H. Cai and Andrew W. Poon, "Optical manipulation of microparticles using whispering-gallery modes in a silicon nitride microdisk resonator," Opt. Lett. **36**(21), 4257–4259 (2011).
21. X. Yang, D. Bao, and B. Li, "Plasmon-Mediated Whispering-Gallery-Mode Emission from Quantum-Dot-Coated Gold Nanosphere," J. Phys. Chem. C **119**(45), 25476–25481 (2015).
22. X. Qu, J. Li, Z. Yin, and H. Zou, "New lithography technique based on electrohydrodynamic printing platform," Org. Electron. **71**, 279–283 (2019).
23. W. Zhou, G. Min, J. Zhang, Y. Liu, J. Wang, Y. Zhang, and F. Sun, "Nanoimprint Lithography: A Processing Technique for Nanofabrication Advancement," Nano-Micro Lett. **3**(2), 135–140 (2011).
24. Y. Zhang, Q. Sun, B. Leung, J. Simon, M. L. Lee, and J. Han, "The fabrication of large-area, free-standing GaN by a novel nanoetching process," Nanotechnology **22**(4), 045603 (2011).
25. M. He, Z. Zhang, S. Shi, J. Du, X. Li, S. Li, and W. Ma, "A practical nanofabrication method: surface plasmon polaritons interference lithography based on backside-exposure technique," Opt. Express **18**(15), 15975 (2010).
26. V. G. Kravets, F. Schedin, and A. N. Grigorenko, "Extremely narrow plasmon resonances based on diffraction coupling of localized plasmons in arrays of metallic nanoparticles," Phys. Rev. Lett. **101**(8), 087403 (2008).
27. S. R. K. Rodriguez, M. C. Schaafsma, A. Berrier, and J. G. Rivas, "Collective resonances in plasmonic crystals: Size matters," Phys. B (Amsterdam, Neth.) **407**(20), 4081–4085 (2012).
28. S. Hong, O. Shim, H. Kwon, and Y. Choi, "Autoenhanced Raman spectroscopy via plasmonic trapping for molecular sensing," Anal. Chem. **88**(15), 7633–7638 (2016).
29. B. Yan, A. Thubagere, W. R. Premasiri, L. D. Ziegler, L. Dal Negro, and B. M. Reinhard, "Engineered SERS substrates with multiscale signal enhancement: Nanoplarticle cluster arrays," ACS Nano **3**(5), 1190–1202 (2009).
30. Y. Z. Shi, H. T. Zhao, K. T. Nguyen, Y. Zhang, L. K. Chin, T. T. Zhu, Y. F. Yu, H. Cai, P. H. Yap, P. Y. Liu, S. Xiong, J. B. Zhang, C. W. Qu, C. T. Chan, and A. Q. Liu, "Nanophotonic array-induced dynamic behavior for label-free shape-selective bacteria sieving," ACS Nano **13**(10), 12070–12080 (2019).

31. R. Hartig, M. Hausmann, J. Schmitt, D. B. J. Herrmann, M. Riedmiller, and C. Cremer, "Preparative continuous separation of biological particles by means of free-flow magnetophoresis in a free-flow electrophoresis chamber," Electrophoresis **13**(1), 674–676 (1992).

32. D. Forge, Y. Gossuin, A. Roch, S. Laurent, L. Vander Elst, and R. N. Muller, "Development of magnetic chromatography to sort polydisperse nanoparticles in ferrofluids," Contrast Media Mol. Imaging **5**(3), 126–132 (2010).

33. F. Bonaccorso, M. Zerbetto, A. C. Ferrari, and V. Amendola, "Sorting nanoparticles by centrifugal fields in clean media," J. Phys. Chem. C **117**(25), 13217–13229 (2013).

34. N.-T. Huang, H. Zhang, M.-T. Chung, J. H. Seo, and K. Kurabayashi, "Recent advancements in optofluidics-based single-cell analysis: optical on-chip cellular manipulation, treatment, and property detection," Lab Chip **14**(7), 1230–1245 (2014).

35. X. Xu, Y. Dong, G. Wang, W. Jiao, Z. Ying, H. P. Ho, and X. Zhang, "Reconfigurable sorting of nanoparticles on a thermal tuning silicon based optofluidic chip," IEEE Photonics J. **10**(1), 1–7 (2018).

36. X. Yang, R. Xu, L. Wen, Z. Lou, Q. Chen, and B. Li, "Light-induced thermal convection for collection and removal of carbon nanotubes," Fundam. Res. **2**(1), 59–65 (2022).

37. R. Quidant, D. Petrov, and G. Badenes, "Radiation forces on a Rayleigh dielectric sphere in a patterned optical near field," Opt. Lett. **30**(9), 1009 (2005).

38. X. Yang, Y. Liu, R. F. Oulton, X. Yin, and X. Zhang, "Optical forces in hybrid plasmonic waveguides," Nano Lett. **11**(2), 321–328 (2011).

39. Y. Zhang, C. Min, X. Dou, X. Wang, H. P. Urbach, M. G. Somekh, and X. Yuan, "Plasmonic tweezers: for nanoscale optical trapping and beyond," Light: Sci. Appl. **10**(1), 1–41 (2021).

40. D. G. Kotsifaki and S. N. Chormaic, "Plasmonic optical tweezers based on nanostructures: Fundamentals, advances and prospects," Nanophotonics **8**(7), 1227–1245 (2019).

41. A. H. J. Yang, T. Lerdsuchatawanich, and D. Erickson, "Forces and transport velocities for a particle in a slot waveguide," Nano Lett. **9**(3), 1182–1188 (2009).

42. E. E. Michaelides, "Brownian movement and thermophoresis of nanoparticles in liquids," Int. J. Heat Mass Transfer **81**, 179–187 (2015).